Effect of substrate on the atomic structure and physical properties of thermoelectric $Ca_3Co_4O_9$ thin films



2011 J. Phys.: Condens. Matter 23 305005

(http://iopscience.iop.org/0953-8984/23/30/305005)

J. Phys.: Condens. Matter **23** (2011) 305005 (6pp) doi:10.1088/0953-8984/23/30/305005

# Effect of substrate on the atomic structure and physical properties of thermoelectric $Ca_3Co_4O_9$ thin films

**Q Qiao[1], A Gulec[1], T Paulauskas[1], S Kolesnik[2], B Dabrowski[2], M Ozdemir[3,4], C Boyraz[3,4], D Mazumdar[3], A Gupta[3] and R F Klie[1]**

[1] Department of Physics, University of Illinois at Chicago, Chicago, IL, USA
[2] Department of Physics, Northern Illinois University, DeKalb, IL, USA
[3] Center of Materials for Information Technology, University of Alabama, Tuscaloosa, AL, USA
[4] Department of Physics, Marmara University, Istanbul, Turkey

Received 15 March 2011, in final form 24 May 2011
Published 1 July 2011
Online at stacks.iop.org/JPhysCM/23/305005

**Abstract**

The incommensurately layered cobalt oxide $Ca_3Co_4O_9$ exhibits an unusually high Seebeck coefficient as a polycrystalline bulk material, making it ideally suited for many high temperature thermoelectric applications. In this paper, we investigate properties of $Ca_3Co_4O_9$ thin films grown on cubic perovskite $SrTiO_3$, $LaAlO_3$, and $(La_{0.3}Sr_{0.7})(Al_{0.65}Ta_{0.35})O_3$ substrates and on hexagonal $Al_2O_3$ (sapphire) substrates using the pulsed laser deposition technique. X-ray diffraction and transmission electron microscopy analysis indicate strain-free growth of films, irrespective of the substrate. However, depending on the lattice and symmetry mismatch, defect-free growth of the hexagonal $CoO_2$ layer is stabilized only after a critical thickness and, in general, we observe the formation of a stable $Ca_2CoO_3$ buffer layer near the substrate–film interface. Beyond this critical thickness, a large concentration of $CoO_2$ stacking faults is observed, possibly due to weak interlayer interaction in this layered material. We propose that these stacking faults have a significant impact on the Seebeck coefficient and we report higher values in thinner $Ca_3Co_4O_9$ films due to additional phonon scattering sites, necessary for improved thermoelectric properties.

## 1. Introduction

Thermoelectric (TE) power applications offer a potentially cheap, pollution- and maintenance-free alternative energy source by converting heat into electricity. This approach relies on scavenging heat from industrial processes or exhaust gases, all of which generate enormous amounts of unused waste heat, and converting it to electricity via the use of TE devices. In particular, TE generators are ideal for small, distributed power generation, since they are solid-state devices with no moving parts, and therefore are silent, reliable and scalable.

While the TE effect has been known for decades, a resurgence of interest in thermoelectrics began in the mid-1990s when theoretical predictions suggested that TE efficiency could be greatly enhanced through nano-structural engineering, which led to experimental efforts demonstrating proof-of-principle high-efficiency materials [1, 2]. At the same time, complex bulk materials (such as skutterudites, clathrates, Zintl phases [3, 4]) were found to achieve high TE efficiencies. In 2001, a benchmark study using nano-structured $Bi_2Te_3$–$Bi_2Se_3$ superlattices showed a TE figure of merit (ZT) of approximately 2.4 at room temperature [5], thereby breaking the threshold for efficiently producing electricity using TE devices. Consequently, the majority of research on TE devices has focused on metastable nano-structures, such as quantum dots, superlattices or nano-wires. However, such systems are unstable at high temperatures, toxic, as well as difficult and expensive to synthesize for large scale applications.

Over the last decade, there has been an increasing number of attempts to synthesize TE oxide materials consisting of elements that are abundant in nature and that will be stable at high temperatures. One such promising material appears to be $Ca_3Co_4O_9$, an incommensurately layered, p-type TE material consisting of rocksalt-type $Ca_2CoO_3$ layers

 

sandwiched between two hexagonal $CdI_2$-like $CoO_2$ layers stacked along the $c$-axis. Both subsystems share the same lattice parameters with $a = 4.8339$ Å, $c = 10.8436$ Å and $\beta = 98.14°$, but along the $b$-axis the incommensurate structure results in $b_1 = 2.8238$ Å for the $CoO_2$ subsystem and $b_2 = 4.5582$ Å for the $Ca_2CoO_3$ subsystem [6]. The triangular $CoO_2$ layer consists of edge sharing oxygen octahedra.

$Ca_3Co_4O_9$ has been shown to exhibit a remarkably high TE figure of merit, ZT, and Seebeck coefficient, $S$, at high temperatures. More specifically, a Seebeck coefficient of nearly 250 $\mu$V K$^{-1}$ and ZT $\sim$ 1 have been measured at 1000 K [7, 8], without any signs of thermal decomposition in air. Therefore, $Ca_3Co_4O_9$ in combination with a stable n-type TE oxide could be used for high temperature energy conversion, using for example engine or industrial waste heat, or even excess heat from concentrator solar cells to generate electrical power.

There have been several models to explain the high Seebeck coefficient in $Ca_3Co_4O_9$, including spin-entropy [9–11], interlayer charge transfer [12, 13] and compressive strain on the $CoO_2$ subsystem [14]. Most importantly, it was recently shown that the different subsystems in $Ca_3Co_4O_9$ fulfil different functions for TE transport [14–16]. The hexagonal $CoO_2$ subsystem can be viewed as a highly p-type doped monolayer and exhibits enhanced two-dimensional conductivity. In fact, a recent study has shown that pristine $CoO_2$ can be described as a metal near a Mott transition for unit-cell parameters of $a = b = 2.806$ Å [17]. The rocksalt $Ca_2CoO_3$ layer on the other hand is insulating, and acts as a charge reservoir, transferring mobile holes into the $CoO_2$ layer. The incommensurate structure of $Ca_3Co_4O_9$ contributes to the overall low thermal conductivity, and additional modulations of the CoO columns in the rocksalt layer have been reported to further reduce the thermal conductivity [18].

Many studies have attempted to further improve the TE properties of bulk $Ca_3Co_4O_9$ using doping, pressure or structural modulations [14, 19]. Another approach that is being explored is to create highly textured or even single-crystal $Ca_3Co_4O_9$ films, exhibiting higher Seebeck coefficients than polycrystalline bulk material, since it is generally believed that grain boundaries negatively affect the TE properties of $Ca_3Co_4O_9$ [14, 16, 19, 20]. However, a detailed study of the films' morphology, in particular, the structure of thin films on substrates with different lattice mismatch and symmetry has not been explored and the effects of interfacially induced strain or film thickness remain unclear.

In this study, we have used the pulsed laser deposition (PLD) technique to deposit $Ca_3Co_4O_9$ thin films on $SrTiO_3$ (STO), $LaAlO_3$ (LAO), $(La_{0.3}Sr_{0.7})(Al_{0.65}Ta_{0.35})O_3$ (LSAT) and $Al_2O_3$ (sapphire) substrates with different film thicknesses and have characterized the structure of the resulting films using x-ray diffraction, high-resolution transmission electron microscopy (TEM) and transport measurements. More specifically, we have studied the effects of lattice mismatch between the substrate and the $Ca_3Co_4O_9$ film, and the change in the Seebeck coefficient as a function of film thickness. We have observed textured and relatively strain-free $Ca_3Co_4O_9$ films on all the above substrates with the $c$-axis of $Ca_3Co_4O_9$ oriented along the growth direction. However, the substrate has a pronounced effect on the hexagonal $CoO_2$ subsystem, which can be stabilized only after a certain thickness of the growing film. Therefore, in the initial growth stages we observe the formation of the rocksalt $Ca_2CoO_3$ 'buffer' layer only, before the full stoichiometric $Ca_3Co_4O_9$ film growth. This effect is particularly striking on cubic substrates where the buffer layer extends to up to 25 nm in thickness, whereas on hexagonal sapphire substrate it is only a few nanometers. We show that in the vicinity of this buffer layer a high concentration of $CoO_2$ stacking faults is formed which act as very efficient phonon scattering sites. As a result, a significant increase in the Seebeck coefficient is observed in films with less than 50 nm thickness.

## 2. Methods

The PLD technique (Coherent Lambda Physik Excimer laser, $\lambda = 248$ nm) was used to prepare the films. The films were grown either on (001)-oriented perovskite-based substrates (STO, LAO, LSAT), or (0001)-oriented $Al_2O_3$ substrates, at a substrate temperature of between 700 and 750 °C and 300 mTorr oxygen pressure. Laser fluence was fixed at 1.5 J cm$^{-2}$ and the repetition rate generally varied between 4 and 8 Hz. The higher rate did not deteriorate the film morphology (as evaluated by x-ray diffraction analysis) and was, therefore, preferred in general. After deposition, all films were cooled down to room temperature in 760 Torr oxygen pressure at a slow rate of 5 °C min$^{-1}$. A standard $\theta$–$2\theta$ four-circle x-ray diffraction (XRD) setup (Phillips X' pert Pro) was used to ascertain the phase and texture of our films. XRD measurements were performed using a Cu K$\alpha$ source operating at 45 kV and 40 mA. Rocking curve (omega scans) measurements were used to quantify the film texture. Film surface morphology was characterized using atomic force microscopy (Veeco NanoScope) scanned in the tapping mode. The sample growth rate per unit pulse was calibrated using the x-ray reflectivity technique. Energy-dispersive x-ray spectroscopy (EDS) was used to determine the film Ca:Co stoichiometry.

The TEM analysis utilized the JEOL3010 at UIC, a conventional $LaB_6$ transmission electron microscope, equipped with a Noran EDS detector and a $1k \times 1k$ Gatan CCD camera. The thin film samples were prepared using conventional cross-sectional methods, including dimpling and ion-beam thinning using Ar-ions at 3 kV.

The in-plane Seebeck coefficient and electrical resistivity measurements were conducted at Northern Illinois University using a physical property measurement system (Quantum Design) equipped with a thermal transport option. Electrically and thermally conductive contacts were made using EPO-TEK® H20E silver epoxy. For the majority of samples, at least four measurements were taken at room temperature on thin film samples with a size of 2.5 mm × 5 mm. The error bars reported here indicate the statistical spread of these measurements. However, to compare our experimental setup with previously published data, we measured the Seebeck coefficient and electrical resistivity of $Ca_3Co_4O_9$ films on glass

**Table 1.** Summary of experimental results for $Ca_3Co_4O_9$ thin films.

| Substrate | Film thickness (nm) | (001) FWHM | *c*-lattice parameter (Å) | Buffer layer thickness (nm) | In-plane lattice mismatch (%) | Seebeck coefficient ($\mu$V K$^{-1}$) |
|---|---|---|---|---|---|---|
| $SrTiO_3$ | 100 | 0.30 | 10.73 | 5–8 | 14.3 | $147.3 \pm 1.5$ |
| $LaAlO_3$ | 100 | 0.23 | 10.74 | 7.0 | 16.9 | $122.9 \pm 0.9$ |
| $LaAlO_3$ | 40 | 0.24 | 10.74 | 7.0 | 16.9 | $144.2 \pm 0.8$ |
| $(La_{0.3}Sr_{0.7})(Al_{0.65}Ta_{0.35})O_3$ | 100 | 0.51 | 10.75 | 25 | 15.2 | $128.5 \pm 1.1$ |
| $(La_{0.3}Sr_{0.7})(Al_{0.65}Ta_{0.35})O_3$ | 40 | 0.31 | 10.75 | 25 | 15.2 | $133.5 \pm 0.8$ |
| $Al_2O_3$ | 100 | 1.17 | | 3.4 | −5.0 | $145.3 \pm 2.2$ |

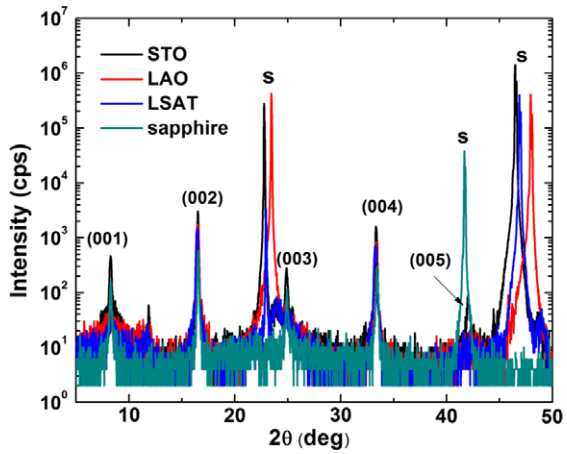


**Figure 1.** X-ray diffraction patterns for $Ca_3Co_4O_9$ thin films grown on $SrTiO_3$, $LaAlO_3$, $(La_{0.3}Sr_{0.7})(Al_{0.65}Ta_{0.35})O_3$, and $Al_2O_3$ substrates in the 5°–50° range showing (00*l*) film reflections. The peaks marked 's' denote substrate peaks.

(This figure is in colour only in the electronic version)

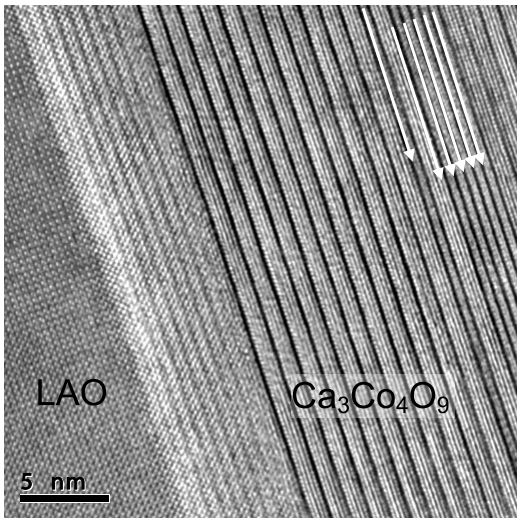


**Figure 2.** High-resolution TEM image of 40 nm thick $Ca_3Co_4O_9$ film on $LaAlO_3$. The location of the $CoO_2$ stacking faults is indicated by white arrows.

as a reference between 15 and 400 K. A comparison with previously published data taken from similar samples [20] shows good agreement of both the Seebeck coefficient and the resistivity within the experimental error bars over the measured temperature range.

## 3. Results and discussion

The XRD measurements are summarized in figure 1 for the different $Ca_3Co_4O_9$ films on LAO (bulk lattice parameter $a$ = 3.798 Å), LSAT ($a$ = 3.866 Å), STO ($a$ = 3.905 Å) and sapphire ($Al_2O_3$, $a$ = 4.785 Å, $c$ = 12.991 Å). Large-angle $\theta$–$2\theta$ scans were obtained from 5° to 90°, showing only diffraction peaks corresponding to (00*l*) $Ca_3Co_4O_9$ film reflections or the substrate. In figure 1, we plot only data between 5° and 50° for better clarity. No evidence of any secondary phases was found. One general feature, irrespective of the substrate, was that the even order reflections ((002), (004), etc) were much sharper and more intense than the odd order reflections ((001), (003), etc). The rocking curve and out-of-plane lattice parameter measurements were performed on the (002) film reflection, which was consistently the strongest diffraction peak for all samples. The summary of the results is shown in table 1. We find the *c*-parameter to be insensitive to the different substrates, and we measured an out-of-plane component of the *c*-lattice parameter of around 10.75 Å for all cubic substrates and at a slightly lower value of 10.70 Å on sapphire. These values are consistent with the bulk *c*-parameter of $Ca_3Co_4O_9$ (10.846 Å), and the monoclinic distortion of ∼98°. Similar values have been previously reported for $Ca_3Co_4O_9$ thin films [19]. Such consistency in *c*-values, coupled with the fact that it is film thickness independent, indicates that the $Ca_3Co_4O_9$ films are growing relatively strain-free.

The film texture has been found to be consistently better on cubic substrates than on sapphire and the full-width-at-half-maximum (FWHM) values obtained on LAO, LSAT and STO substrates are between 0.3° and 0.5°, while the films on sapphire substrates show an FWHM value of over 1.0°. These results, namely the strain-free growth and better texture on cubic substrates, are consistent with our TEM analysis, which is presented next.

We have studied the microstructure of $Ca_3Co_4O_9$ thin films grown on cubic oxide substrates, with increasing lattice parameters. Figure 2 shows the TEM micrograph of a 100 nm thick $Ca_3Co_4O_9$ film on (001)-oriented LAO substrate (lattice constant 3.79 Å), with a nominal lattice parameter mismatch between the substrate and the unstrained $Ca_3Co_4O_9$ of 16.9%. This film exhibited the best x-ray rocking curve FWHM and film texture. The high-resolution TEM micrograph (figure 2)

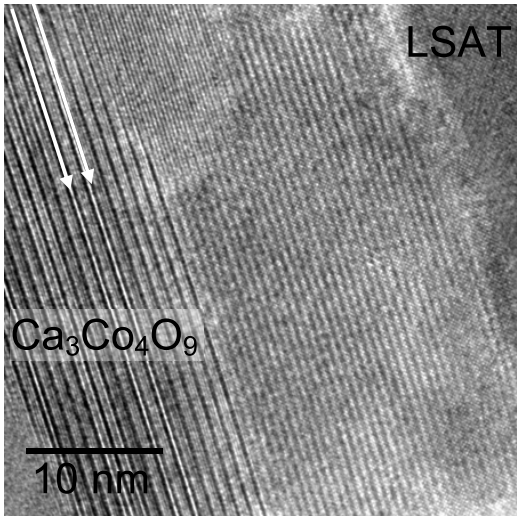


**Figure 3.** High-resolution TEM image of 100 nm thick $Ca_3Co_4O_9$ film on $(La_{0.3}Sr_{0.7})(Al_{0.65}Ta_{0.35})O_3$. The location of the $CoO_2$ stacking faults is indicated by white arrows.

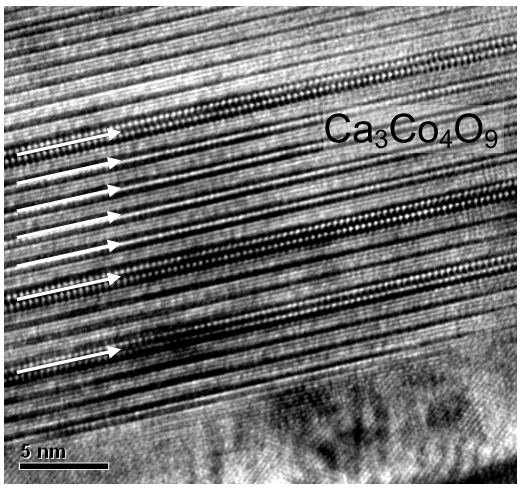


**Figure 4.** High-resolution TEM image of 100 nm thick $Ca_3Co_4O_9$ film on $SrTiO_3$. The location of the $CoO_2$ stacking faults is indicated by white arrows.

shows the LAO substrate on the left in the [001] orientation and the $Ca_3Co_4O_9$ film on the right. The layered structure of the $Ca_3Co_4O_9$ can be clearly seen as periodic dark lines. However, between the $Ca_3Co_4O_9$ film and the LAO substrate, a buffer layer is clearly visible, exhibiting cubic symmetry and then a sharp transition to the $Ca_3Co_4O_9$ film. Based on our EDS/electron energy loss spectroscopy (EELS) analysis, we propose that the buffer layer consists of cubic $Ca_2CoO_3$, and is 7 nm thick throughout the area characterized in this study. In addition to the buffer layer, we find that a high density of $CoO_2$ stacking faults exists in the first 20–30 nm of the $Ca_3Co_4O_9$ film. It is interesting to note here that while the *c*-axis of the LAO substrate and the $Ca_3Co_4O_9$ are well aligned, there appears to be some degree of in-plane rotation of the film to further accommodate the residual lattice mismatch.

To further examine the effect of film thickness on the film microstructure, strain and TE properties, we have investigated the properties of a 50 nm thick $Ca_3Co_4O_9$ film on LAO. We found that the microstructure in the thinner films is similar to the thicker films shown in figure 3, with a 7 nm rocksalt buffer layer and a high density of stacking faults in the vicinity of the substrate/film interface. However, the Seebeck coefficient for the films of different thicknesses (table 1) shows a significant increase for thinner films on LAO. More specifically, the Seebeck coefficient at room temperature in the 100 nm thick film was found to be $122.9 \pm 0.9$ $\mu$V K$^{-1}$ (comparable to the bulk sample) while that of the 50 nm thick film increased to $144.2 \pm 0.8$ $\mu$V K$^{-1}$. Similarly, the electrical resistivity of the films increased from $23.1 \pm 0.1$ m$\Omega$ cm for the 100 nm thick film to $27.3 \pm 0.1$ m$\Omega$ cm for the 50 nm thick film.

Figure 3 shows the TEM micrograph of a nominally 40 nm thick $Ca_3Co_4O_9$ film grown on (001) LSAT (lattice constant 3.866 Å). Although both the diffraction pattern (figure 1(a)) and the rocking curve suggest a highly textured growth along the *c*-axis, and a film quality similar to the films on LAO, it is apparent in the TEM image that the buffer layer thickness is significantly larger than in LAO. We have measured a buffer layer thickness of 20–30 nm, and we again observe stacking faults in the vicinity of the buffer layer/$Ca_3Co_4O_9$ film interface. In the case of the 40 nm thick films, the effective $Ca_3Co_4O_9$ film thickness is only 10–20 nm, and the $CoO_2$ stacking faults now penetrate all the way to the film surface. The Seebeck coefficient for the 100 nm thick samples is $128.5 \pm 1.1$ $\mu$V K$^{-1}$, and shows only a moderate increase to $133.5 \pm 0.8$ $\mu$V K$^{-1}$ in the 40 nm thick films. The room temperature electrical resistivity was measured at $55.5 \pm 0.1$ m$\Omega$ cm and $20.9 \pm 0.1$ m$\Omega$ cm for the 100 and 40 nm thick films, respectively, again suggesting a strong dependence of the resistivity as a function of films thickness.

Films on STO (001) substrate also show a similar trend. Figure 4 shows a TEM micrograph of a 100 nm thick $Ca_3Co_4O_9$-film on STO. The STO substrate is shown as the dark area at the bottom of figure 4, which clearly shows the $Ca_2CoO_3$ buffer layer between the STO substrate and the layered $Ca_3Co_4O_9$ films. The thickness of this buffer layer is measured to be between 5 and 8 nm thick. Near the $Ca_2CoO_3$/$Ca_3Co_4O_9$ interface, we again find a large density of $CoO_2$ stacking faults that show up as the white dotted lines in figure 4. These stacking faults continue up to a film thickness of about 20–30 nm from the buffer layer. The 100 nm thick $Ca_3Co_4O_9$ films grown on STO exhibit the highest Seebeck coefficient measured in this study with $S_{STO} = 147.3 \pm 1.5$ $\mu$V K$^{-1}$, while the electrical resistivity at room temperature is measured at $34.7 \pm 0.1$ m$\Omega$ cm.

A number of previous studies have reported high quality film synthesis on $Al_2O_3$ substrates, but also the presence of secondary phases and out-of-plane grain rotation. In our study, the $Ca_3Co_4O_9$ films grown in sapphire (figure 5) exhibit many features similar to the films grown on STO, e.g. textured growth along the *c*-axis of $Ca_3Co_4O_9$ and large, single phase grains. However, there are several distinct differences that can be found in the films grown on sapphire compared to any of the other films grown on cubic substrates. Firstly, the buffer layer thickness is on average 2–3 nm, much smaller

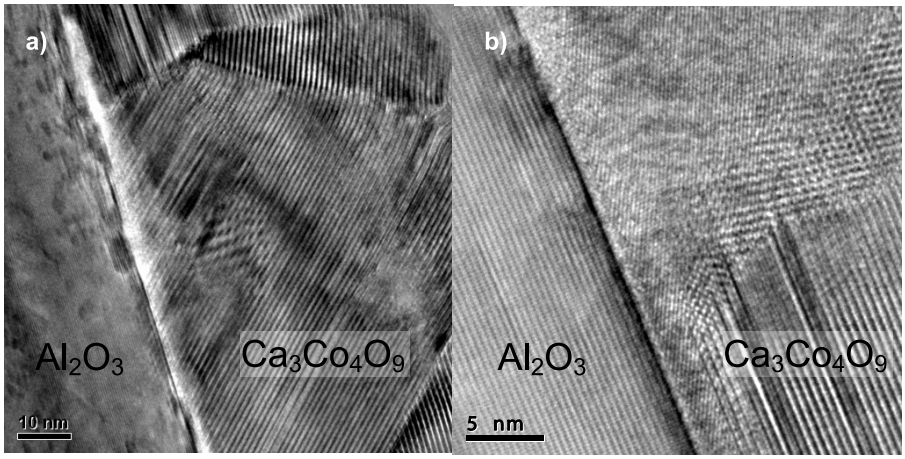


**Figure 5.** High-resolution TEM image of 100 nm thick $Ca_3Co_4O_9$ film on $Al_2O_3$.

than what is observed on cubic substrates. However, we observe distinct areas where the grains are rotated which also affects the buffer layer thickness. Figure 5(a) shows one region of the 100 nm $Ca_3Co_4O_9$ film on sapphire that exhibits this interesting orientation of the $Ca_3Co_4O_9$ films. While the top of the image shows the $Ca_3Co_4O_9$ film with the *ab*-plane parallel to the film/substrate interface, there appears to be a part of the $Ca_3Co_4O_9$ film where the *ab*-plane of $Ca_3Co_4O_9$ is 70° inclined with respect to the interface. It seems that the buffer layer thickness changes as a function of grain orientation, with the grains in the (001) orientation exhibiting the thickest buffer layer (3–4 nm thick), and a sharp transition from the sapphire substrate to the film is found for the grains that show a rotation similar to that shown in figure 5(a).

Figure 5(b) shows a TEM image of another region in the $Ca_3Co_4O_9$/sapphire sample with a distinct buffer layer between the $Ca_3Co_4O_9$ film and the sapphire substrate. The buffer layer thickness was measured to be between 2 and 3 nm. In addition to $Ca_3Co_4O_9$, we find a number of smaller grains with a lattice parameter of 5.0 Å (top of figure 5(b)), which we attribute to $Ca_xCoO_2$. Growth of the $Ca_xCoO_2$ phase with a lattice parameter of 5.4 Å has been reported under similar growth conditions [18], suggesting that these grains are formed due to lack of sufficient oxygen or rapid film growth rate and exhibit no notable TE properties [21]. It is interesting to note here that the Seebeck coefficient of the $Ca_3Co_4O_9$ film on sapphire is similar to that of the film on STO ($S_{\text{sapphire}} = 145.3 \pm 2.2\ \mu\text{V K}^{-1}$), in spite of the broader x-ray rocking curve and the presence of secondary phases and misoriented $Ca_3Co_4O_9$ grains. However, the resistivity at room temperature was measured at $68.3 \pm 0.1$ mΩ cm, higher than the value on STO substrate.

While the precise physical reason for the observation of the buffer layer is not easily explained, it is clear that the buffer layer appears to relieve the interfacial strain without the formation of any point defects at the film/buffer layer interface. In addition, an in-plane rotation of the $Ca_3Co_4O_9$ film with respect to the substrate appears to be relieving the remaining strain in the films. Also, there are strong reasons to hypothesize that the substrate symmetry mismatch plays a crucial role in the formation of the buffer layer. $Ca_3Co_4O_9$ has both a cubic ($Ca_2CoO_3$) and hexagonal ($CoO_2$) layers, and based on the thickness of the buffer layer, we can generally say that the cubic $Ca_2CoO_3$ layers are relatively easily stabilized, compared to the hexagonal $CoO_2$. This effect is particularly pronounced on cubic substrates and close to the substrate/film interface (where the substrate effect is expectedly large). On hexagonal sapphire the buffer is significantly thinner, implying that layers of both symmetry (particularly the hexagonal $CoO_2$ layer) can be stabilized close to the substrate. However, the thickness of the buffer layer cannot be explained from lattice mismatch alone, which is not surprising as the lattice mismatch values are already very large (well over 10%). The non-equilibrium growth kinetics of the PLD technique could also play a significant role, but the understanding of this effect is beyond the scope of the present work. Nevertheless, irrespective of the substrate, we observe that the growth of $CoO_2$ ensues with a large number of stacking faults near the $Ca_2CoO_3$ buffer layer/$Ca_3Co_4O_9$ film interface, which at times permeate all the way to the film surface. To explain this, it is worth commenting that this layered material is held together by weak interlayer (possibly van der Waals) forces, similar to other layered materials, such as graphite and boron nitride. Since the difference in energy between the possible stacking sequence is small, it can be easily overcome in a non-equilibrium thin film growth process (like PLD, for example) leading to the observed stacking faults. The creation of $CoO_2$ stacking faults appears to coincide with a higher Seebeck coefficient and lower electrical resistivity of the $Ca_3Co_4O_9$ films. It was previously shown that the $CoO_2$ subsystem in $Ca_3Co_4O_9$ is responsible for the electrical conductivity and high TE transport, while the rocksalt subsystem is acting as a charge reservoir [12]. The formation of double $CoO_2$ layers within the $Ca_3Co_4O_9$ matrix should therefore result in an increase in the Seebeck coefficient and a decrease in the electrical resistivity, as observed in our study. The formation of stacking faults could also stabilize degenerate spin states, which leads to greater spin-entropy and a large Seebeck coefficient as a consequence [11].

The observed thickness dependence of the Seebeck coefficient further confirms our hypothesis that the occurrence

of $CoO_2$ stacking faults is responsible for the increased Seebeck coefficient in thinner $Ca_3Co_4O_9$ films, since the majority of stacking faults is observed in the vicinity of the $Ca_3Co_4O_9$ film/$Ca_2CoO_3$ buffer layer interface. However, there appears to be a limit to that claim, as seen in the 40 nm thick $Ca_3Co_4O_9$ films on LSAT. For films which mostly consist of non-TE $Ca_2CoO_3$, the high density of $CoO_2$ in $Ca_3Co_4O_9$ does not result in a net increase in the film's Seebeck coefficient. Overall, it appears that the $Ca_3Co_4O_9$ films grown on STO exhibit the best TE and electrical properties. Although no $Ca_3Co_4O_9$ films on STO with less than 100 nm thickness were characterized in this study, it appears possible to further increase the Seebeck coefficient of the $Ca_3Co_4O_9$ films by reducing the film thickness to 40–50 nm.

The effect of stacking faults on the phonon scattering rate has been modeled previously in other layered materials, such as cuprate superconductors [22], and it has been shown that the scattering rate is proportional to the number of stacking faults per unit length, which is in qualitative agreement with our measurements on films with different thickness. That is why it is not surprising that films with the higher Seebeck coefficient and lower electrical conductivity show relatively inferior texture. Future studies will examine the effects of grain boundaries and secondary phases on the $Ca_3Co_4O_9$ films' transport properties.

In summary, we report that the atomic structure of $Ca_3Co_4O_9$ thin films is significantly different compared to polycrystalline samples, which has a considerable effect on the TE properties. Based on the film properties grown on different substrates, we conclude that a combination of the lattice and symmetry mismatch, combined with the non-equilibrium growth kinetics, determines the $Ca_3Co_4O_9$ thin film structure. The hexagonal $CoO_2$ layers of $Ca_3Co_4O_9$ are particularly difficult to stabilize at the initial growth stage on cubic substrates, and as a result a buffer layer of cubic $Ca_2CoO_3$ layer is observed in all our films near the substrate. Further, a large number of $CoO_2$ stacking faults is observed near this buffer layer, which we primarily attribute to the weak interlayer attraction between the layers. The formation of the $CoO_2$ stacking faults has significant impact on the Seebeck coefficient, acting as phonon scattering sites, and we observe a moderate enhancement in the Seebeck coefficient values on thinner, more disordered films. Based on the results presented in this paper, there appear to be several ways to further increase the TE properties of $Ca_3Co_4O_9$: while the substrate induced strain does not seem to directly affect the Seebeck coefficient or lattice parameters of $Ca_3Co_4O_9$, the creation of $CoO_2$ stacking does. Therefore, controlled synthesis of $CoO_2$ stacking faults within $Ca_3Co_4O_9$ thin films appears to be one method of increasing the Seebeck coefficient without negatively affecting the electrical conductivity.

## Acknowledgments

This research was supported by the US Army Research Office under contract number W911NF-10-1-0147 and the National Science Foundation (DMR-0846748). The authors would also like to thank the UIC Research Resources Center, in particular Drs A W Nicholls and K B Low for their help. TP also acknowledges support from the Sivananthan Undergraduate Research Fellowship.

## References

[1] Dresselhaus M S, Chen G, Tang M Y, Yang R G, Lee H, Wang D Z, Ren Z F, Fleurial J P and Gogna P 2007 *Adv. Mater.* **19** 1043–53
[2] Chen G, Dresselhaus M S, Dresselhaus G, Fleurial J P and Caillat T 2003 *Int. Mater. Rev.* **48** 45–66
[3] Nolas G S, Poon J and Kanatzidis M 2006 *MRS Bull.* **31** 199–205
[4] Kauzlarich S M, Brown S R and Snyder G J 2007 *Dalton Trans.* 2099–107
[5] Venkatasubramanian R, Siivola E, Colpitts T and O'Quinn B 2001 *Nature* **413** 597–602
[6] Miyazaki Y, Onoda M, Oku T, Kikuchi M, Ishii Y, Ono Y, Morii Y and Kajitani T 2002 *J. Phys. Soc. Japan* **71** 491–7
[7] Funahashi R, Matsubara I, Ikuta H, Takeuchi T, Mizutani U and Sodeoka S 2000 *Japan. J. Appl. Phys.* 2 **39** L1127–9
[8] Shikano M and Funahashi R 2003 *Appl. Phys. Lett.* **82** 1851–3
[9] Wang Y Y, Rogado N S, Cava R J and Ong N P 2003 *Nature* **423** 425–8
[10] Koshibae W and Maekawa S 2001 *Phys. Rev. Lett.* **87** 236603
[11] Koshibae W, Tsutsui K and Maekawa S 2000 *Phys. Rev.* B **62** 6869–72
[12] Yang G, Ramasse Q and Klie R F 2008 *Phys. Rev.* B **78** 153109
[13] Yang G, Ramasse Q and Klie R F 2009 *Appl. Phys. Lett.* **94** 093112
[14] Matsubara I, Funahashi R, Shikano M, Sasaki K and Enomoto H 2002 *Appl. Phys. Lett.* **80** 4729–31
[15] Xu G J 2002 *Appl. Phys. Lett.* **80** 3760–2
[16] Hu Y F, Si W D, Sutter E and Li Q 2005 *Appl. Phys. Lett.* **86** 082103
[17] de Vaulx C, Julien M H, Berthier C, Hebert S, Pralong V and Maignan A 2007 *Phys. Rev. Lett.* **98** 246402
[18] Muguerra H, Grebille D and Bouree F 2008 *Acta Crystallogr.* B **64** 144–53
[19] Sun T, Hng H H, Yan Q Y and Ma J 2010 *J. Appl. Phys.* **108** 083709
[20] Hu Y F, Sutter E, Si W D and Li Q 2005 *Appl. Phys. Lett.* **87** 171912
[21] Kanno T, Yotsuhashi S and Adachi H 2004 *Appl. Phys. Lett.* **85** 739–41
[22] Tewordt L and Wölkhausen T 1989 *Solid State Commun.* **70** 839–44